Article

Experimental Study on the Agglomeration Behavior of Elongated Biomass Particles in a Lifting Tube

Mingpu Du, Junjie Yang, Ye Tao, Bingyang Xu, Conghui Gu,* Haichao Zhao, Yuan Liu, Kaiyuan Deng, and Jingyu Zhu

Read Online

ACCESS | Metrics & More | Article Recommendations

ABSTRACT: Pneumatic conveying devices are commonly used in the fields of chemical industry, raw material transportation, and material processing. Elongated biomass particles are not evenly distributed in the lifting tube because biomass clumps during conveying. Pneumatic conveying test setup and measurement system were built in this paper in order to study the agglomeration behavior of elongated biomass particles in the lifting tube experimentally. Particle tracking velocimetry (PTV) was used to determine the area distribution and velocity distribution of particles at different apparent air velocities and mass flow rates. The results show that while keeping the mass flow rate constant at 46.50 g/s, the apparent gas velocity increased from 5.91 to 7.91 m/s and the maximum size of agglomerates decreased from 0.689 to 0.235. The apparent gas velocity was kept at 6.40 m/s, and the particle mass flow rate was adjusted from 56.50 to 16.20 g/s. The maximum size of the agglomerates was reduced to 0.115. Therefore, appropriately increasing the apparent gas velocity or decreasing the particle mass flow rate can improve the uniformity of the particle distribution in the lifting tube. The results would provide a reference for parameter adjustment of pneumatic conveying devices in industrial production.
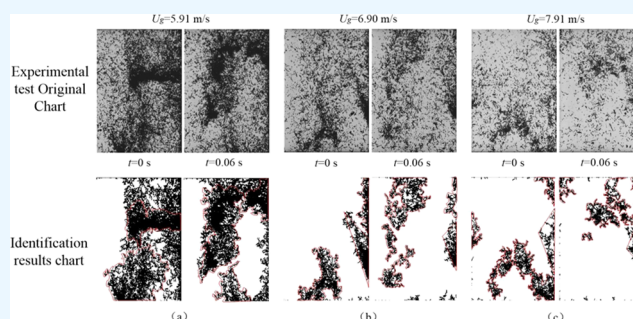
1. INTRODUCTION

With the realization of mankind that the use of traditional energy sources has had a serious impact on the environment and climate change, the use of clean energy has received increasing attention from countries around the world.[1−3] As a kind of green, low-carbon, and clean energy, biomass can be widely used in industry, life, transportation, and other fields.[4−6] In biomass energy, the pneumatic conveying device is an efficient gas−solid reaction and heat and mass transfer equipment, which has many advantages, such as fast gas−solid transfer speed, high contact efficiency, and high utilization of raw materials and equipment.[7−9] Therefore, pneumatic conveying devices are widely used in the conversion process of biomass energy, which makes an essential contribution to the development of the clean energy industry.[10−13] After nearly 70 years of fundamental theoretical research and technological development, pneumatic conveying devices are now widely used in many industries, such as the chemical industry, energy, food processing, material processing, environmental protection, and so on.[14−18] Some of the advantages of pneumatic conveyors are the low number of moving parts, flexible setup, and fully enclosed transportation, all of which create environmentally safe applications.[19] It serves not only as an alternative for transporting pellet materials

between locations or blending different pellet types but also facilitates the prefabrication of biomass pellets, offering functionalities such as moisture content control, sorting, feed, and mixing.[20−22] In the realm of contemporary engineering applications, there is a prevailing preference for dilute-phase conveying, which proves to be the most economical mode due to the inherent ease of cleaning and maintenance associated with the equipment compared to concentrated-phase conveying systems.[23] During system operation, the conversion of energy generated in the braking process into electricity allows for effective energy recovery, contributing to a reduction in the overall energy consumption of the system.[24] This adaptation aligns well with the demands of sustainable development.
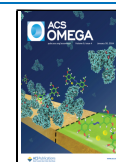
Although the pneumatic conveying device, as an efficient gas−solid reaction and heat and mass transfer equipment, has many functions, such as material conveying, drying, and

processing, there are still some shortcomings. Among them, handling materials with uneven moisture content and materials with special shapes is particularly problematic. Specifically: (1) As a result of the uneven residence time of biomass feedstock in the conveying device during processing, the moisture content of some materials is too high or too low, which affects the quality and yield of biomass products. The biomass drying process also requires attention to energy consumption and equipment maintenance. These issues can increase the water content in the development, thus affecting the efficiency of biomass drying and the stability of product quality.[25] (2) Materials with unique shapes (such as filamentary biomass particles) have structural characteristics such as being easy to bend and can be entangled, which in the conveying and drying process is very likely to lead to particles sticking to each other and agglomeration.[26] Thereby, reducing the contact efficiency between the material and the gas-phase medium affected the drying effect. Some national and international scholars have visualized the parameters such as shape and size, residence time, and speed of movement of particle agglomerates.[27] The results of all of the studies have shown that the contact efficiency of the gas-solid phases and the flow behavior of the particles have a significant impact on the performance of the lift tube reactor.[28−30] In this regard, some scholars have proposed relevant experimental research methods. Wilhelm and Kwauk[31] were the first to observe particle aggregation fluidization, where particles aggregate into groups and move together in a conventional fluidized bed. Yerushalmi et al.[32] observed that the particles aggregated in chains and clusters under rapid fluidization. He[33] used the PIV method to capture the agglomerates at the lifting tube and obtain the magnitude and direction of the particle motion velocity. Zha[34] used a coupled LBM-DEM model to study the settling pattern of particles under three-dimensional conditions. The results showed that when particles are higher, the particle settling process is more likely to have agglomeration between particles. Deng[35] used the K-means clustering algorithm to cluster the grayscale maps of transient particle distributions obtained from Wang et al.[36] simulations, and was able to clearly capture the core agglomerates in the lifting tubes and the cloud of particles surrounding the core of the agglomerates. Liu and Lu[37] used the Eulerian−Lagrangian method to predict the behavior of cluster populations in circulating fluidized bed lift tubes. The simulation results show that new clusters can be formed in the near-wall area and transferred from the near-wall region to the riser core. Based on the literature, Ullah[38] defined the size of dimensionless axial clusters. The experimental acquisition of cluster size and its distribution was conducted, and a comparison was made with the empirical correlations available in the literature. The results show that the calculations of the existing methods are in good agreement with the available data. Sharma et al.[39] suggested that the particle concentration within the particle floc should be greater than twice the standard deviation of the change in particle concentration plus the local mean particle concentration. Mondal et al.,[40] on the other hand, used mean grayness and grayness standard deviation to determine particle clusters. Soong et al.[41] proposed three criteria that agglomerate need to fulfill: (1) The concentration of agglomerates should be significantly higher than the time-averaged particle concentration at the same operating parameters; (2) concentration fluctuations caused by agglomerates should be greater than the average pulsation in particle concentration; (3) the size of the agglomerates shall be greater

than 100 particle diameters. Sun,[42] in his study on the identification and behavior of quartz sand, agglomerates with an average particle size of $d = 0.25$ mm, proposed that white areas identified as containing or less than three pixels were considered as discrete particles, and white areas containing three or more pixels were considered as particle flocs. Shi[43] conducted PIV tests on the velocity distribution of different particles within a bubbling fluidized bed using a self-built PIV system for flow characterization of circulating fluidized beds. Particle clusters were found to have a significant effect on the gas−solid flow behavior within the bed. Sun[42] developed an image acquisition and processing system for three-dimensional visualization of fluidized bed rising tubes. Particle flocs formed by quartz sand with an average particle size of $d = 0.25$ mm were investigated, and it was found that the method was able to accurately identify "U"-shaped, inverted "U"-shaped, and bar-shaped particle clusters. Verma[23] used a high-speed video camera in his experiments to acquire nonspherical particles in a pneumatic conveying system with dilute-phase transport polarization, and the study shows that the difference in particle size affects segregation significantly.

Gas−solid phase flow is very complex[44] and encompasses interactions between the fluid phase and the solid phase as well as between the solid phase and the solid phase. Current measurement techniques for collecting data within a flow field are usually: pressure transducers and hydrostatic probes for measuring pressure in a flow field; Raman scattering spectroscopy technique for the measurement of gas molecules in flow fields; sensor temperatures measurement techniques such as thermocouples, thermistors, thermal imaging cameras, infrared thermometers, and other devices that can monitor temperature changes in real time;[45] laser Doppler velocimetry, laser photography, holographic technology, PIV (Particle Image Velocimetry) technology, etc.[46] These methods can measure flow velocities, flow characteristics, particle aggregation, and more. The flow within the flow field is a moving process that changes constantly, and noncontact measurement techniques are mostly chosen for the measurement process. These measurement techniques can measure the distribution of various parameters within the flow field, and it is changing law without interfering with the movement of the object, thus providing reliable experimental data to provide strong support for the study of the dynamic characteristics of the flow field. Lackmeier et al.[47] proposed a method to visualize the internal structure of pilot CFB risers using laser sheet and image processing techniques. Wu[48] used a high-speed camera and image processing techniques to study the motion of nonspherical particles inside the lifting tube. By analyzing the relationship between the area of connected domains of particles and the number of connected domains, the domain area of 9000 pixels is used as a threshold to distinguish small clusters from large clusters. Lu[49] employed high-speed camera and image acquisition techniques to record the particle agglomeration behavior and its dynamic motion process in the lifting tube. The results show that the trajectory of the agglomerates in the lifting tube is consistent with the "ring-nucleus flow" model. The vertical velocity of the agglomerates is distributed horizontally in an approximately symmetrical manner with "high center and low sidewalls". Yang and Zhu[50] propose a new image processing method based on image calibration in the study of visualizing clusters in the fully developed region of a Plexiglas rectangular circulating fluidized bed (CFB) lifting tube. As a result, high Gs and low U_g favor

the formation of clusters with high solids content, while low Gs and high U_g lead to the rupture of clusters. The findings presented above are of great significance for designing gas—solid fluidization systems and studying flow mechanisms.

In recent years, visualization methods have become increasingly popular with the development and improvement of high-speed cameras and the application of image processing techniques. An overview of the practical applications of conventional industrial measurement techniques is given in the literature described above, which discusses more complex localized measurement techniques within multiphase flow devices that have demonstrated their applicability in large industrial reactors. In this paper, we record the motion of nonspherical particle clusters in the lifting tube by means of a self-constructed cold pneumatic conveying experimental setup with a PTV measurement system. Applying a high-speed camera in the pneumatic conveying practical system enables visualization studies. To ensure the recognition's accuracy, the results are compared with the original image to get a suitable range of calculation thresholds. The focus of this study introduces the parameters of agglomerate size (dimensionless number φ), velocity distribution, and velocity variance to deal with and quantitatively analyze the agglomerate behavior inside the lift tube. The agglomeration behavior and distribution uniformity of the particle population in the lifting tube under different working conditions were investigated. The introduction of the dimensionless parameter of the cluster size adds more universality to the conclusions.

2. EXPERIMENTAL MATERIALS AND METHODS

2.1. Experimental Materials and Devices. Nonspherical filamentous biomass particles were used as experimental materials, as shown in Figure 1. The average length of the

Figure 1. Elongated biomass particles.

elongated biomass particles was 1.22 cm, the width was about 1.0 cm, and the actual density was about 450 kg/m³. Nine points were sampled after the material was spread uniformly on a flat surface, as shown in Figure 2. About 4 g of elongated biomass material was taken from each sampling cassette and placed in the oven. At a temperature of 100 °C baking,[51] until the quality of the sampling box does not change, several experiments measured the baking time of 3 h appropriate. The dried elongated biomass particles were placed in a desiccator and left for 1 h. The dried elongated biomass particles were placed in a desiccator for 1 h. Its mass after drying was finally
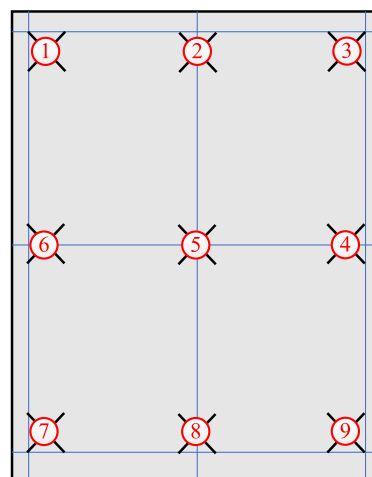

Figure 2. Schematic diagram of sampling points for measuring water content of materials.

measured and then the moisture content of the wet base was calculated to be about 19.2%, and the moisture content was calculated as shown in eq 1[51]

$$W = \frac{m_1 - m_2}{m_1} \tag{1}$$

where W is the moisture content of the wet base, %; m_1 is the mass of the material specimen before drying, g; and m_2 is the mass of the model dried in the oven at 100 °C to a constant weight, g. The importance of the specimen before drying, m_2, is the mass of the sample dried at 100 °C to a stable weight.

Figure 3 shows a schematic diagram of the experimental system, which consists of a pneumatic conveying system and an image acquisition and processing system. The pneumatic conveying system consists of a blower, an unloading device, a screw feeder, a lifting tube, a return tube, and a cyclone separator. The height of the fluidized bed pipe is 58.0 cm, and the cross section is a rectangle of 20.5 cm × 12.8 cm made of acrylic. Its light transmittance is good, easy to maintain, more environmentally friendly, and easy to photograph and observe the flow state of the particle population in the bed during the experiment. The image acquisition and processing system consists of a high-speed CCD camera (Charge Coupled Device), LED panel light source, fill light, and image processing system. A high-speed CCD camera captures images of elongated biomass particles moving through the lifting tube. The panel light source is placed on the back wall of the lift tube. The panel light source is diffusely reflected to form a uniform irradiation light in the lifting tube, which can increase the brightness of the shooting area by 20−50%. Compared with the fill light front illumination method, using a panel light source can effectively reduce the appearance of image shadows so that the captured particle group motion picture is more accurate and precise. The fill light supplements the light during the shoot to ensure the area is well-lit. Thus, a higher-quality image is obtained, and the image data can be analyzed and processed by the image processing system to obtain the relevant parameters of particle motion.

2.2. Experimental Methods and Conditions. Before conducting the biomass nonspherical pellet movement experiments, the pellets need to be homogeneously mixed to avoid affecting the results of the experiments due to excessive local
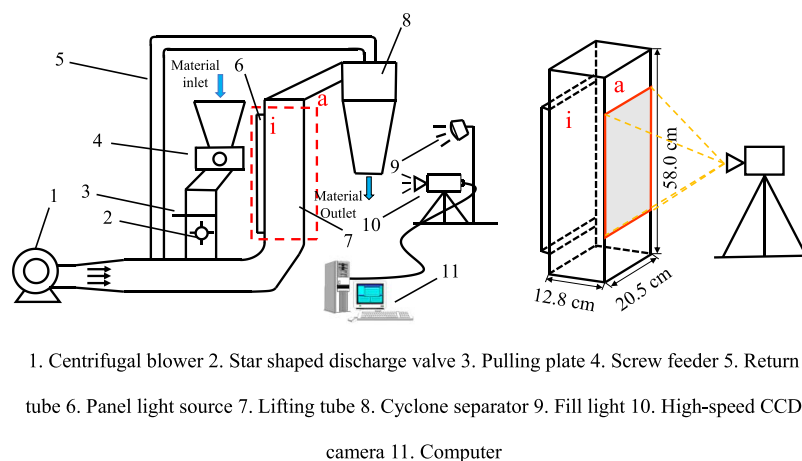
1. Centrifugal blower 2. Star shaped discharge valve 3. Pulling plate 4. Screw feeder 5. Return tube 6. Panel light source 7. Lifting tube 8. Cyclone separator 9. Fill light 10. High-speed CCD camera 11. Computer

Figure 3. Schematic diagram of pneumatic conveying experimental system.

differences in moisture content. After mixing, the shots are stored in the hopper of the screw feeder, and the granules are charged using the screw feeder and star-shaped discharge valve. A variable frequency motor controls the speed to ensure continuous feeding during the experiment. The star-shaped discharge valve can continuously feed particles into the pneumatic conveying unit at a constant flow rate.

At the start of the test, the centrifugal blower must be switched on and the inverter must be adjusted so that the airflow is evenly distributed in the ducting. When the airflow is stabilized, the release of the particles is initiated, and the video image is captured after the screw feeder is able to stabilize the feed. The particles are fed into the pipeline through the star-shaped discharge valve and then pass through the air supply pipe and lifting tube before finally reaching the cyclone for gas−solid separation. The gas is returned to the experimental device through the return duct for recycling. At the end of the experiment, the captured video needs to be transferred to a computer processing system for data processing and analysis, such as analyzing the speed, trajectory, particle cluster area, and other parameters of particle movement. The proper execution of the above steps helps ensure the experiment's stability and obtain more accurate results.

The high-speed CCD camera model 5F04 M used in the experiments has a full-frame resolution of 2320 × 1720 (500 fps) and a small-frame speed of up to 52,800 fps. To ensure the quality and accuracy of the shooting and to accurately record the experimental data, several experiments were conducted, and it was found that shooting at a frame rate greater than 905 frames shortened the shooting If the shooting frame rate is less than 900 frames, it will reduce the quality of the picture and increase the error of postprocessing data. Therefore, the experimental shooting for a more appropriate shooting frame rate of 902 frames was selected. The actual dimensions of the capture surface "a" of the lifting tube are 20.5 cm × 58.0 cm, as shown in Figure 3, and the capture window is chosen to minimize the influence of the inlet and outlet on the particle motion in the lifting tube. After the wall thickness of 1.5 cm on both sides is excluded, the cross-sectional dimensions of the lift tube are 9.8 cm × 17.5 cm. Therefore, the actual size of the viewfinder window was chosen to be 17.5 cm × 20.5 cm, between 13.5 cm from the lift tube outlet and 13 cm from the inlet. The specific information is detailed in Table 1. When the airflow is stabilized, the release of the particles is initiated, and the video image is captured after waiting for the screw feeder

Table 1. Data Acquisition Shooting Parameters

parameters	numerical
emitting area	40 cm × 30 cm
acquisition window	768 pixel × 940 pixel
actual window size	17.5 cm × 21.5 cm
lift tube cross-sectional dimensions	9.8 cm × 17.5 cm
plotting scale	4.4
capture frame rate	902 frames
shooting duration	7 s
exposure time	40 μs
aperture size	F/11

to stabilize the feed. In order to study the motion law of biomass nonspherical particles in the lifting tube under different working conditions, ten groups of experimental conditions were set up in this study, and the effects of air velocity and particle mass flow rate on the uniformity of particle motion and agglomeration behavior were investigated, respectively. Specific information on the experimental conditions is detailed in Table 2. The design of these experimental

Table 2. Experimental Study Working Conditions

apparent gas velocity/(m·s^{-1})	mass flow rate/(g·s^{-1})
5.91	46.50
6.40	46.50
6.91	46.50
7.43	46.50
7.91	46.50
6.40	16.20
6.40	26.00
6.40	36.50
6.40	46.50
6.40	56.50

conditions is reasonable and practicable, which can effectively analyze the motion characteristics of particles under different conditions and provide critical experimental data and references for further research on the transport motion of nonspherical particles.

3. IMAGE RECOGNITION AND DATA PROCESSING

3.1. Image Background Segmentation Threshold X. This study used the background gray level threshold
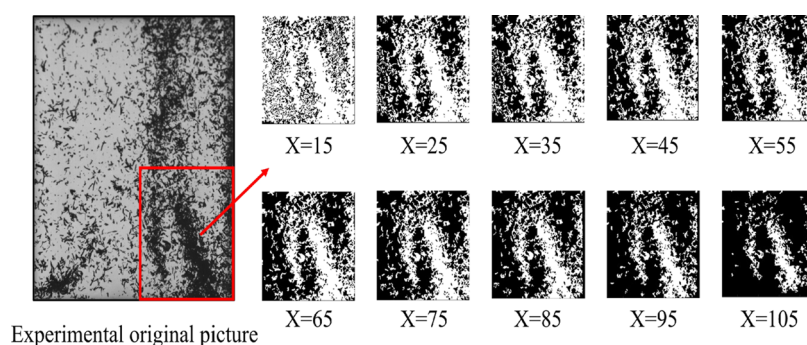
Figure 4. Comparison of recognition results of particle clusters with different background segmentation thresholds X.
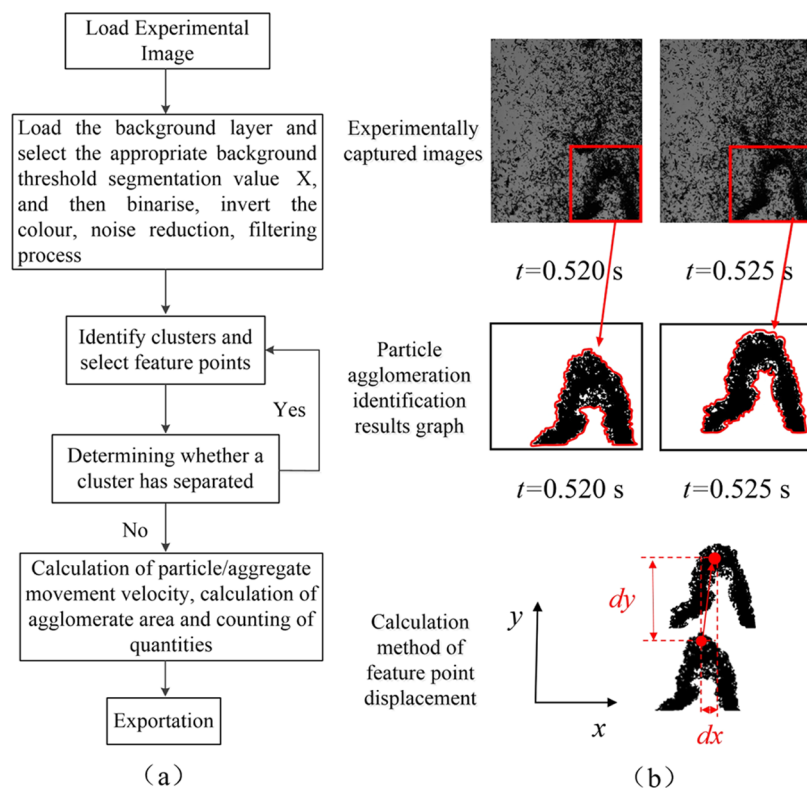

Figure 5. (a) Flowchart of particle cluster feature point selection. (b) Schematic diagram of particle agglomeration identification and velocity calculation (U_g = 6.40 m/s, M_s = 46.50 g/s, dt = 0.005 s).

segmentation method to process captured motion images of elongated biomass particles. The brief operation principle is as follows: first, background segmentation threshold X is set, which is used to determine whether the recognized targets in the image are discrete particles or agglomerates. When a target is identified, the portion of the target with a gray value more significant than X is determined by the algorithm to be a cluster of particles (discrete particle clusters or agglomerates). In contrast, the portion of the target with a gray value less than the preset value of X is considered to be the background. The white region was obtained as part of the final identified nonspherical particle agglomerates by binarization, noise reduction, and inverse color processing methods of the image. According to different experimental environments and needs, the background segmentation threshold X value can be adjusted to quickly and accurately identify the nonspherical particle agglomerates of raw materials and their internal structures. This method is characterized by its simplicity,

effectiveness, and reproducibility. It is suitable for different types and scales of biomass particle movement experiments and provides primary data for the biomass transport process research.

To determine the appropriate background segmentation threshold X value and to accurately identify the clustered morphology of the nonspherical particles of the birth material. This study conducted comparative experiments on the recognition of elongated biomass particle clusters under different background segmentation thresholds. The results are shown in Figure 4. According to the red region comparison chart; the analysis indicates that the recognition results under the three thresholds of X = 65, 75, and 85 are more consistent with the original graph. Compared to the experimental results with segmentation thresholds of 65 and 85, the recognized particle clusters are closer to the actual experimental images when the segmentation threshold is 75; however, when the segmentation threshold is ≤65, too low of a segmentation

threshold can cause some of the black areas around the recognized particle clusters to also be determined to be part of the particle cluster. And when the segmentation threshold $X \geq$ 85, the segmentation intensity is too large, and the lower gray value at the edge of the nonspherical particle cluster is also recognized as the background, which leads to the incomplete recognition of the particle cluster. This is consistent with Yin's conclusions in identifying the effects of different k values used in the k-means algorithm.[52] Taken together, the segmentation threshold $X = 75$ (± 5) was chosen in this study to accurately identify the clustered morphology of nonspherical particles of birth matter. This paper analyzes the uniformity of particle distribution and the law of agglomerate shape evolution by observing the changes of elongated biomass particle clusters at different moments with working conditions.

3.2. Velocity Recognition Operations for Particle Agglomerates.

For the study of the motion of particles in the lifting tube, three methods for calculating the particle agglomeration velocity are commonly used today: (1) The outer boundary displacement method.[49] The displacements and rates of the particle aggregates are calculated by measuring the exiles at the outer boundary of the particle aggregates. (2) Center of mass displacement method.[39] The displacement and velocity of the granular agglomerates were obtained by calculating the removal of the center of mass of the granular agglomerates. (3) Particle tracking velocimetry.[50] In other words, a certain number of points are selected in the length direction of a single flexible nonspherical particle, and the motion characteristics of the elastic nonspherical particle are obtained by measuring the translational and nontranslational motions of these points. Due to the complexity of the particle flow in the pneumatic conveying device and the variability of the size and structure of the particle agglomerates, this study has chosen to analyze the motion of the particle agglomerates by selecting the characteristic point displacements. The specific particle aggregation feature point selection process is shown in Figure 5a. In addition, to recognize the information on particle agglomerates, this study uses the background segmentation thresholding method using image processing. Figure 5b shows the particle agglomeration identification and velocity calculation schematic diagram. For example, the image of a particle agglomerate converging in the lifting tube at the experimental conditions: $U_g = 6.40$ m/s, $M_s = 46.50$ g/s, and $t = 0.520$ s. The image of a particle agglomerate joining the lifting tube at the experimental conditions: $U_g = 6.40$ m/s and $M_s = 46.50$ g/s. The background segmentation thresholding method first obtains information about particle clusters. Afterward, a feature point is randomly selected, and the motion of the particle agglomerates is tracked by the position of the feature point within the particle agglomerates before the agglomerates are separated. If the cluster scatters into multiple clusters, the algorithm will reselect the feature points to avoid the change of feature point locations. When the particle clusters are clustered from small clusters into larger clusters, the algorithm performs cross-correlation between consecutive frames of images. Based on the peak values of the cross-correlation, the algorithm identifies new cluster targets, thus selecting the characteristic point.

When performing experimental data processing, since the quality of imported experimental images is often rough, batch improvement processing of the original images is required. The specific processing steps are as follows: first, load the background layer and select the appropriate background

threshold segmentation value X. The grayscale difference between the particles and the background is then enhanced by binarization, inversion, noise reduction, and filtering. In this case, the black and white gray values are 0 and 255, respectively. This move facilitates the division of particles and backgrounds into different regions and provides an excellent environment for image segmentation. The next step in data analysis is performed after the particles or aggregates have been identified. In this study, two frames of images at $t = 0.520$ s and 0.525 s were selected for the operation demonstration, and the velocity V of the particles or particle agglomerates was calculated by calculating the displacements in the x. Y directions of the selected feature points in the period of d$t = 0.005$ s, and in this way, the velocity V of the particles or particle agglomerates was calculated by using the following formulas

$$v = \frac{dy}{dt} \tag{2}$$

$$u = \frac{dx}{dt} \tag{3}$$

$$V = \sqrt{v^2 + u^2} \tag{4}$$

where dx is the displacement of the selected feature point in the x-direction during the period; dy is the displacement of the selected feature point in the y-direction during the period; and dt is the set time difference.

3.3. Statistics on the Number of Granular Aggregates.

When the interaction forces between particles are strengthened, they promote a tighter bonding between the particles, forming agglomerates. When the interaction forces between particles and gas increase, particles experience stronger gravitational or other interactive forces, leading them to tend to aggregate. Conversely, when the particle−particle or particle−gas mutual forces are reduced, the particles are more easily dispersed. This agglomeration phenomenon results in the formation of larger-sized clusters of particles, commonly referred to as a particle cluster. If, when the particles are already aggregated into clusters, the clusters are subjected to greater shear forces exerted on them by the gas, then the clusters may be broken up and dispersed. Particle agglomeration is a common phenomenon in gas−solid two-phase flows. And different methods of particle agglomeration studies will yield different results for the size and number of agglomerates. In this study, an identified target was considered an agglomerator when its pixels were more significant than or equal to three times the average pixel value of a single particle with a minimum agglomeration area of 0.4 cm^2. Those smaller than three times the average pixel value of a single particle are considered individual elongated particles or smaller discrete clusters of particles and are removed by the algorithm. Figure 6 shows the size distribution of cluster connectivity domains, and the number of connectivity domains decreases sharply when the particle cluster size is more significant than 0.012, where the cluster size is calculated according to eq 5. Since most of the particles in the lifting tubes are in the form of discrete particles or small-sized agglomerates, this paper distinguishes between small-sized agglomerates and large-sized agglomerates with a connectivity domain size threshold of 0.012, which is one of the innovations of this study. The study of particle agglomerates provides a better understanding of the flow characteristics of gas−solid two-phase flow in pneumatic
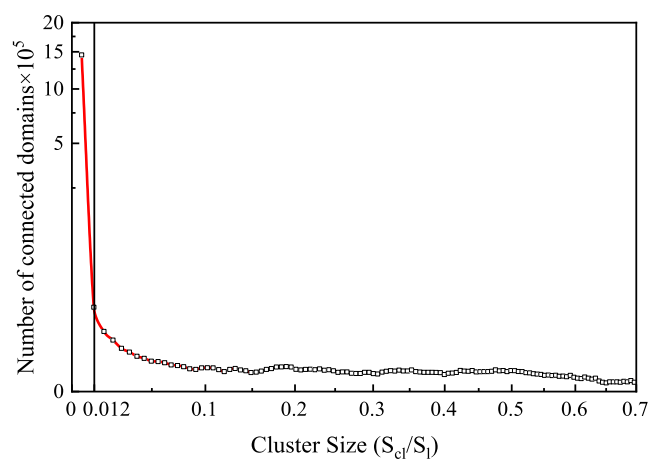
Figure 6. Size distribution of cluster connectivity domains.

4.1. Effect of Apparent Gas Velocity on Cluster Size Distribution. Figure 7 shows the size distribution of particle

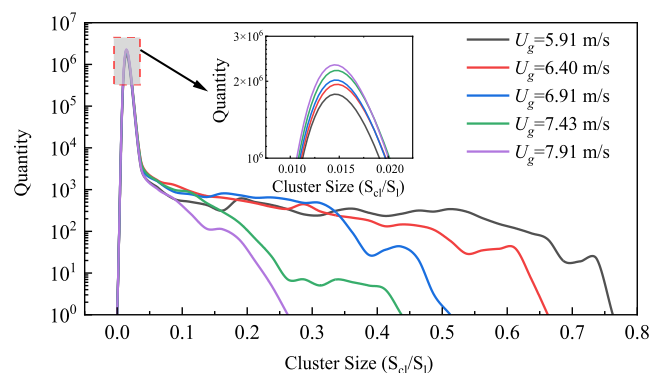**Figure 7.** Size distribution of particle agglomerates with different apparent gas velocities.

conveying, which is essential for optimizing and controlling the pneumatic conveying process.

$$\varphi = \frac{S_{cl}}{S_l} \tag{5}$$

where S_{cl} is the area of the cluster and S_l is the cross-sectional area of the lifting tube.

First, in this paper, the number of clusters is defined in terms of the number of occurrences of clusters in the images of all frames in any given period. To achieve an accurate count of the number of agglomerates, the pixel-area method is used in this article to determine the pixel size of the particle agglomerates and convert it to the area size. After the information about all of the particle clusters in each image frame is identified, the cluster pixel size is converted to an area size using a corresponding scale. Due to the disruptive nature of the conveying equipment during the experimental process, particles smaller than the size of a single particle are removed using a threshold value. Counting the number $n_{k_{s_i \sim s_{i+1}}}$ of clusters with an area size interval of $S_i \sim S_{i+1}$. Eventually the total number N_{S_i} of clusters within the 6314 image frames with the cluster area size interval $S_i \sim S_{i+1}$ can be calculated by a cyclic procedure. This statistical method can more accurately reflect the number and size distribution of particle agglomerates in the lift tube, which helps to analyze the influence of particle agglomerates on the behavior of gas—solid two-phase flow in the lift tube. At the same time, the method can also provide a reference for other studies of particle agglomeration in gas—solid two-phase flow.

$$N_{s_i} = \sum_{k=1}^{6314} n_{k_{s_i \sim s_{i+1}}} \tag{6}$$

where k denotes the number of frames and i is the area size ($i = 0, 1, 2, 3...$).

4. RESULTS AND DISCUSSION

In this section, the effect of apparent gas velocity and mass flow rate on the size of agglomerates in the lift tube is discussed. The uniformity of particle motion in the lift tube under different operating conditions is analyzed in conjunction with the velocity variance s^2 of the particles and the velocity distribution plots.

clusters at different apparent gas velocities, and the area intervals corresponding to the peak number of particle clusters size at five different apparent gas velocities are all 0−0.012. This is because although agglomeration of biomass non-spherical particles occurs in the lifting tube, the vast majority are discrete particles. It is worth noting that the aggregation of biomass nonspherical particles in the lifting tube is most obvious relative to the other four groups when the mass flow rate $M_s = 46.50$ g/s and the apparent gas velocity $U_g = 5.91$ m/s. The maximum cluster size at this apparent air velocity is 0.689 when the air velocity is small enough to blow the material completely into the lifting tube. After particle-to-particle entanglement and collision, as well as particle-to-wall collision, the kinetic energy of the particles decreases and the velocity decreases, resulting in increased entanglement and collision with the particle population blowing from below and an increase in the size of the agglomerates, as shown in Figure 9a. This is similar and consistent with the conclusions obtained from Zhao's simulations.[53] Therefore, with a specific mass flow rate and a small gas velocity, the phenomenon of nonspherical particles aggregating into a large agglomeration is very likely to occur. This phenomenon affects the flow characteristics of the bed gas, which affects the performance of the pneumatic conveying device.

The maximum size distribution of particle agglomerates at five different apparent airflow velocities is shown in Figure 8. When the apparent gas velocity is increased from $U_g = 5.91$ m/s to $U_g = 7.91$ m/s in a gradient of every 0.5 m/s, the number of large-sized agglomerated fraction is decreasing rapidly. The increase in gas velocity increases the shear force of the gas in the tube on the particles. The particles are subjected to more vital shear forces, reducing the probability of aggregation between particles. An increase in the number of small-sized agglomerates and discrete particles accompanies the decrease in the number of large-sized agglomerates. Therefore, the peak height of the number of clusters distributed in 0.012 in the cluster size distribution curve corresponding to $U_g = 7.91$ m/s is the highest group compared to the remaining four groups of working conditions. The air velocity increased by 2 m/s, and the maximum size of the agglomerates was 0.235, which was reduced to about 1/3 of its original size. Therefore, it can be predicted that by increasing the apparent gas velocity, the probability of accumulation of the elongated biomass particle
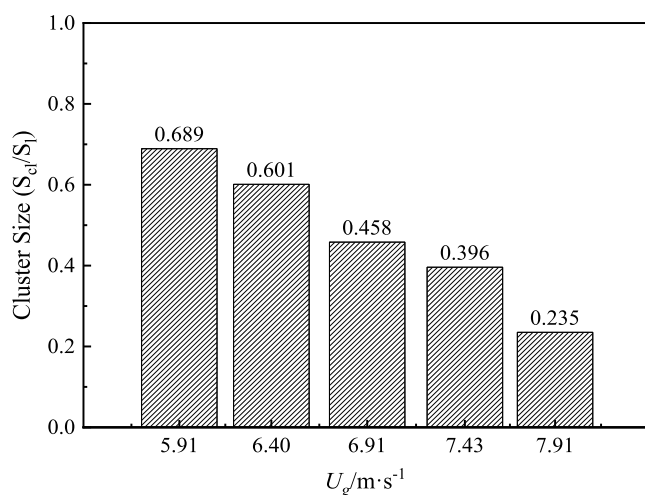
Figure 8. Distribution of maximum agglomeration size of particles at different apparent gas velocities

population in the lifting tube will decrease and the size of the agglomerated particles will be further reduced.

The process of blowing and aggregating particle agglomerates for the three airflow velocities is given in Figure 9. In this paper, we delineate the smallest cluster area as 0.4 cm². When referring to Figure 9, our focus lies in capturing the cluster fragmentation and aggregation processes. Consequently, it becomes imperative to exclude diminutive clusters, which are approximately 1−2 times the size of the smallest cluster. Through scale conversion, 1200 pixels equates to approximately 0.61. To present the process more clearly, the deletion threshold in the image processing code was adjusted to 1200 pixels. Biomass nonspherical particles in the lifting tube, in addition to collision and mutual entanglement to form clusters, at the same time, clusters are blown apart into several small clusters or discrete groups of particles phenomenon. These clusters or agglomerates of discrete particles recollide with the material around them, eventually forming new agglomerates. This process is repeated until the particles reached the top of the lifting tube and are conveyed out. This phenomenon of agglomerates being blown apart and then agglomerating is an essential manifestation of particle flow characteristics, which reflects the strength of the interparticle interaction forces and the interparticle interactions. It also illustrates that the accumulation of particles within a complex and variable airflow field constantly changes, which can have different effects on granular materials during pneumatic conveying. Particle clusters in the lift tube have lower velocities than those blown in at the lift tube inlet due to mutual collisions with the wall or between particles. At the same time, the particles are blown into the lifting tube with higher speeds and collide violently with the particles inside the tube; therefore, the elongated biomass particles are more likely to be aggregated into larger-sized agglomerates at the bottom of the lifting tube. And this aggregation is more pronounced at lower apparent gas velocities.

Comparing the plots of the agglomeration and fragmentation process of particle clusters at different apparent air velocities in Figure 9, the blowing and dispersing ability of the airflow on the particle clusters in the tube is enhanced as U_g is increased from 5.91 to 7.91 m/s. The particle clusters were dispersed into multiple small clusters and discrete particles. And the degree of blown apart becomes more significant with the increase of apparent gas velocity; the higher the apparent gas velocity, the more significant the difference between the shape of the blown apart cluster and the original cluster. Discrete particles and small agglomerates blown apart continue to collide with surrounding particles or agglomerates as their velocity increases due to their freedom from the large-size agglomerates. As shown in Figure 9b,c, "inverted U-shaped" irregular and "triangular" clusters are observed at higher apparent gas velocities. Since the speed of the particles in the sidewall region is significantly smaller than that near the center, the particles settle along the sidewalls and reflux occurs. This is similar and consistent with the findings of Geng[54] and Chen.[55] The tendency of particle aggregation to form agglomerates is different for different spatial locations of the lifting tube. Agglomerates are developed in greater numbers and for a longer period in the sidewall area than in the center area and in more significant numbers. And the location of the experiment where the reflux phenomenon occurred is consistent with Geng's conclusions. Particle reflux at the side walls and particle fragmentation in the near-center area along the airflow direction result in "inverted U-shaped" and "triangular"
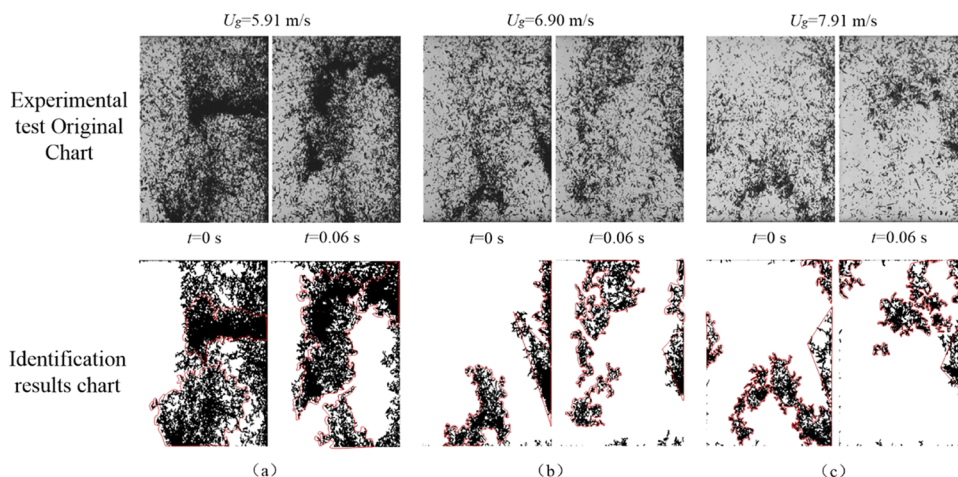

Figure 9. Plot of agglomerate fragmentation and aggregation processes at different apparent gas velocities (deletion threshold: 1200 pixels): (a) U_g = 5.91 m/s, (b) U_g = 6.90 m/s, (c) U_g = 7.91 m/s.

accumulations in the near-wall area. The ability of the airflow to break up the agglomerates is enhanced as the airflow speed increases, so it can be seen that an appropriate increase in the speed of the airflow can promote a better dispersion of particles in the lifting tube, significantly reducing the probability of the emergence of large-sized agglomerates and thus improving the performance of the pneumatic conveying device.

4.2. Effect of Airflow Velocity on the Velocity Distribution of Particle Population. Figure 10 shows the
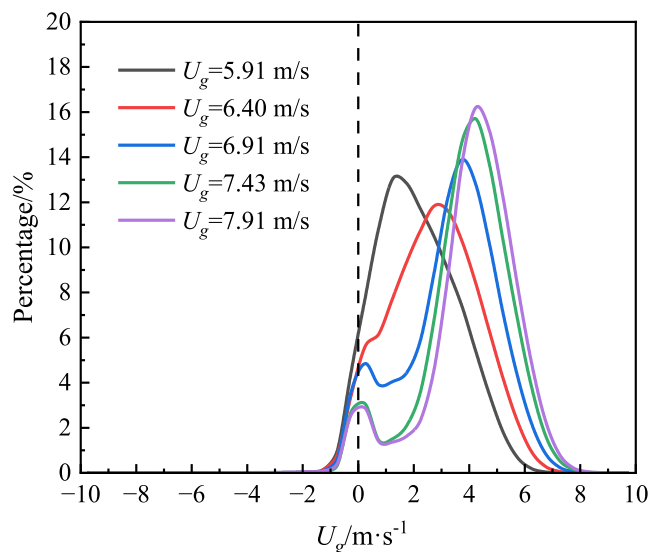

Figure 10. Velocity distribution curves of the particle population at different apparent gas velocities.

velocity distribution profiles of particles at five different airflow velocities for the mass flow rate M_s = 46.50 g/s. When $U_g \geq$ 6.40 m/s, the velocity distribution curve of the particle population gradually shows an apparent bimodal phenomenon. Most of the particle population moves at a higher velocity, and a small portion of the particle population moves at a lower rate. Although most of the particles in the lifting tube are clusters of smaller particles, a small proportion are in the form of large-sized agglomerates. Thus, the first wave peak on the left side of the curve in the figure is the peak number corresponding to the velocities of larger-sized agglomerates. In contrast, the second wave peak is the peak number corresponding to the rates of smaller groups of discrete particles or small-sized agglomerates. When the apparent gas velocity gradually increases, the large-sized particle agglomerates are fragmented into a large number of small-sized particle clusters so that the double peak becomes more and more obvious with the increase of gas velocity. At U_g = 5.91 m/s, the airflow velocity is small at this time, and a large number of agglomerates with larger sizes occur in the lifting tube. Hence, the peak number of particles is low and the velocity distribution curve does not show an apparent double peak. The particle population velocity distribution curve has a negative region with a distribution between −2 and 0 m/s. It is caused by a small amount of backflow occurring on both sides of the lifting tube's wall surface.

The airflow velocity gradually increased, and the rate corresponding to the peak of the velocity distribution curve of the particle population increased from 1.0−1.5 to 4.0−4.5 m/s. As the airflow velocity grows at an isotropic rate of 0.5 m/

s, the growth rate of the peak of the particle velocity distribution curve decreases and the double peak of the curve becomes more and more pronounced. The peak of the velocity distribution curve is shifted to the right. In contrast, the value of the span of the second peak gradually becomes smaller and the velocity difference between particles decreases. This phenomenon is due to an increase in the air velocity; the large size of the agglomerate is blown into several small size particles agglomerates and discrete particles, and the part of the blown part of the large size of the agglomerate as a result of detachment, their speed of movement increased significantly. Increasing the apparent air velocity increases the rate of rise of the particles in the lift tube and decreases the time that the particles remain in the tube. And higher apparent gas velocities reduce the interaction time between the particles and the gas, resulting in a more homogeneous distribution of the particles' velocities, showing a more concentrated velocity distribution. The particle population velocity distribution curve's negative value domain decreases due to the apparent gas velocity increase. This is because increasing the apparent gas velocity increases the gas flow rate in the gas−solid mixture, resulting in some of the particles being rapidly carried away from the lift tube by the gas flow and reducing the particle concentration in the tube. Lower particle concentrations lessen the opportunity for particles to collide and aggregate with each other, thus reducing the probability of aggregation of particles as well as reducing the degree of particle reflux.

Therefore, an appropriate increase in air velocity of 1−2 m/s during the experimental process can increase the movement speed of the particles in the lifting tube and bring the particles out of the lifting tube quickly. Higher apparent gas velocities can improve the homogeneity and stability of the gas flow and reduce local velocity fluctuations and inhomogeneities, leading to a more concentrated and homogeneous particle velocity distribution. And the velocity of the particles tends to be uniform, and the degree of particle cluster reflux will be reduced.

4.3. Effect of Mass Flow Rate on Cluster Size Distribution. The experimental conditions were set at an apparent gas velocity U_g = 6.40 m/s and a mass flow M_s of 16.20−56.50 g/s, which was increased in steps of 10 g/s. Figure 11 shows the size distribution of particle clusters at five different mass flow rates, and the size range of the clusters at the peak number of particle clusters at different mass flow rates is distributed from 0 to 0.012. This finding reaffirms that elongated biomass particles are overwhelmingly present as
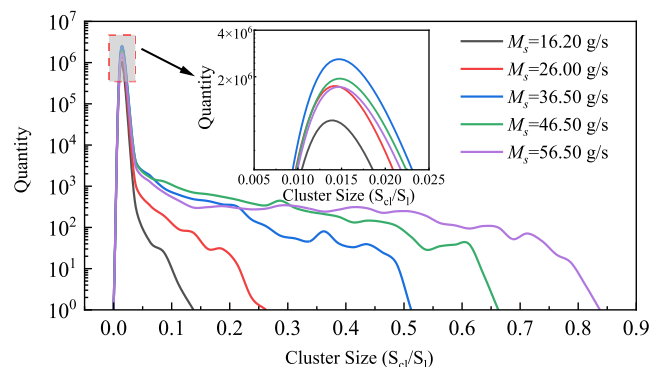

Figure 11. Size distribution of particle agglomerates at different mass flow rates.

small-sized particle clusters in the lift tube. Among them, when the mass flow rate is 36.5 g/s, the number of agglomerates with the size of 0−0.012 is the largest. This is due to the gradual increase in the number of particles. The particles in the lifting tube are still mainly in the size range of 0 to 0.012. When the mass flow rate exceeds 36.5 g/s, the agglomeration of the particles becomes more and more pronounced. Despite the increasing mass flow rate, more groups of particles of small sizes tend to aggregate into agglomerates of larger sizes. So compared to the mass flow rate of 56.50 g/s, the number of agglomerates with size 0−0.012 is more when the mass flow rate is 36.50 g/s. The maximum size of particle agglomeration was 0.115 when the mass flow rate M_s = 16.20 g/s. Due to the small mass flow rate in this set of experiments, the particles were distributed more dispersed inside the lifting tube and did not appear too large but generally existed as a cluster of particles with a size of 0−0.03. The maximum value of 0.753 was reached for the size of particles converging into agglomerates in the lifting tube at M_s = 56.50 g/s, as shown in Figure 12. The results of this study show that the formation
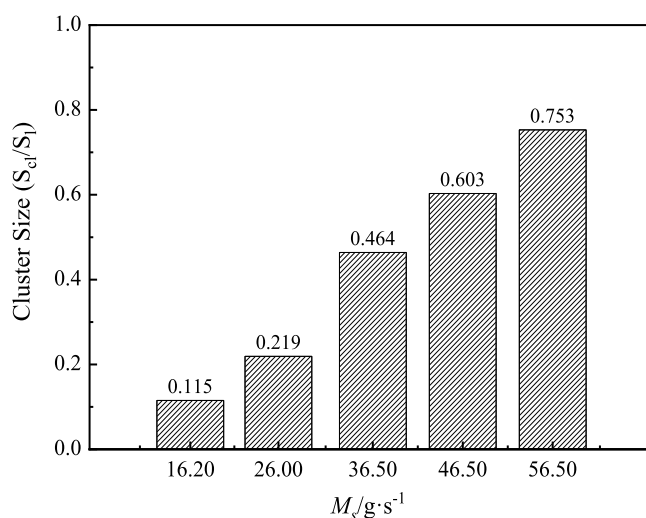

Figure 12. Distribution of the maximum agglomeration size of particles at different mass flow rates.

and aggregation of particle clusters are progressively enhanced as the mass flow rate increases. In addition, the agglomerate area distribution curve may also reflect the size and number of particle agglomerates. The size and number of particle clusters can be quantified and compared by analyzing the size distribution curves of the groups of particles converging into clusters.

In a lifting tube with limited space, the magnitude of particle concentration under the same conditions becomes one of the critical factors affecting the state of motion of particles in the lifting tube. By adjusting the mass flow rate of particles at the inlet, it is possible to change the concentration of particles in the lifting tube. It was shown that by increasing the mass flow rate of particles at the inlet, the clustered size distribution curve of the particle population gradually becomes more expansive. The size of the clusters is moving toward larger sizes, and the number of more significant parts of the cluster size is increasing with it. This is because increasing the mass flow rate at the inlet results in a larger concentration of particles in the lift tube, which increases the chances of particles colliding and aggregating with each other. The experimental materials

used in the experiment were elongated biomass particles prone to random deformation; therefore, higher particle concentrations would make it easier for particles to become entangled with each other and form agglomerates of larger size. It is interesting to note that the size distribution curves of particle cluster clusters in the range of 0−0.012 show that the number of clusters increases and then decreases with increasing particle mass flow rate. The peak of the curves is gradually shifted to the right. The mass flow rate is low at M_s = 16.20 g/s, so the number of particles in the lift tube is low, most of which are clusters of smaller-sized particles. As the mass flow rate gradually increased to M_s = 36.50 g/s, the number of particles in the lift tube also gradually increased. When M_s > 36.50 g/s, the number of particles within the lift increases, but the occupied rate of the pipe cross-sectional area increases, causing the interparticle voids to decrease. Increased interparticle interaction forces result in particles coming together more readily to form agglomerates. In contrast, smaller discrete particles or single particles are blown along with the airflow to form larger agglomerates. Thus, the number of particles in the range of 0−0.012 decreases with increasing mass flow rate, whereas the number of larger-sized agglomerates increases as M_s > 36.50 g/s.

4.4. Effect of Mass Flow Rate on Particle Population Velocity Distribution. The velocity distribution curves of the particle swarm for five different mass flow rates at U_g = 6.4 m/s are given in Figure 13. It can be seen that for the same
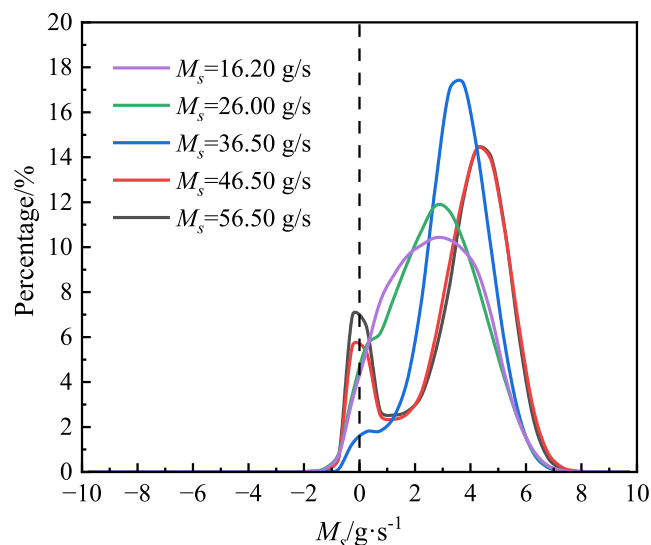

Figure 13. Velocity distribution profile of particle swarms at different mass flow rates.

apparent gas velocity, with an increase in the mass flow rate of the particles, the velocity distribution curve of the particle population in the lifting tube becomes gradually narrower. The curve distribution is wider when M_s = 16.20 g/s when the mass flow rate at the inlet is small, and the particle concentration in the lift tube is low. Therefore, under the experimental condition of U_g = 6.4 m/s, the apparent gas velocity significantly affects particle motion, resulting in a sparse distribution of particles in the lifting tube. Although not pooled into larger agglomerates, the velocity difference between particles becomes larger at larger airflow velocities. Experimentally increasing M_s in steps of every ten g/s up to 36.50 g/s, it was observed that the velocity distribution curve of the
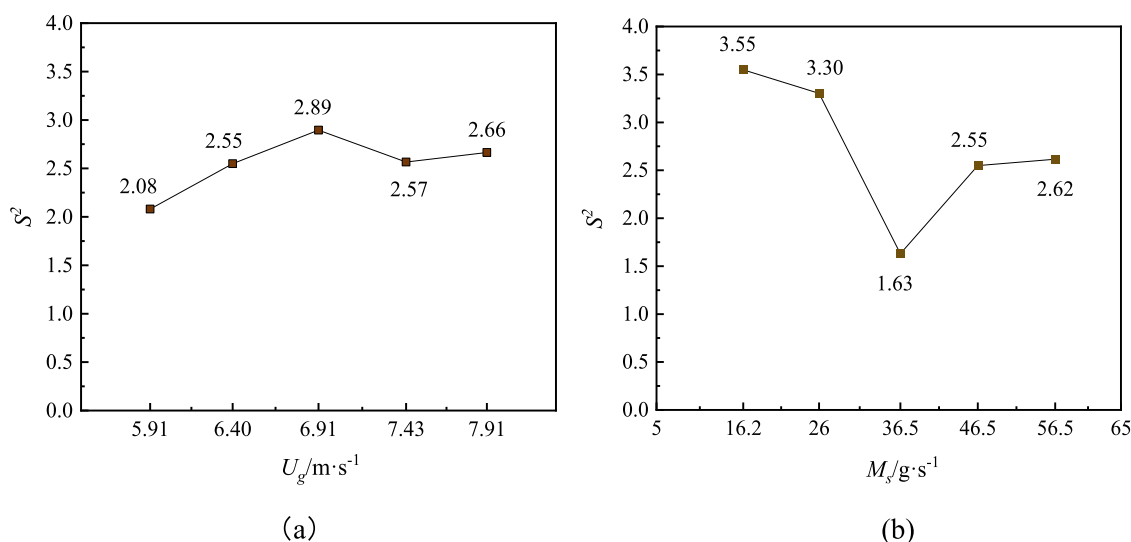
Figure 14. Velocity variance distribution of particle population under different experimental conditions: (a) M_s = 46.50 g/s, (b) U_g = 6.40 m/s.

particle population corresponding to the working conditions became gradually narrower, and the height of the distribution between −2 and 0 m/s decreased. This indicates that the difference in velocity between the particles is falling and the phenomenon of reflux is decreasing. The velocity distribution curve of the particle population shows a clear double peak as the mass flow rate increases after M_s > 36.50 g/s. This is mainly due to the broadening of the distribution of particle group velocities between −2 and 0 m/s, indicating that particle reflux is intensifying in these two sets of experimental conditions. The change of the particle reflux phenomenon occurs mainly at the side walls of the lift tube. The phenomenon of biomass pellets agglomeration and reflux at the side walls of the lifting tube increases the residence time of the pellets in the tube, which tends to directly affect their utilization.

The number distribution curves of the particle population in different velocity intervals show a trend of increasing and then decreasing with the mass flow rate increase. When the mass flow rate is low, increasing M_s enhances the number of particles in the tube, and the peak number of particle populations corresponding to the experimental conditions will be increased accordingly. Further increasing the mass flow rate causes the particles to collide more aggressively with each other and become more likely to become entangled. In contrast, smaller discrete particles or single particles are blown along with the airflow and attached to the cluster to form larger clusters. Therefore, in the experiments with M_s > 36.50 g/s for both sets of conditions, the number of identified particle clusters from 0 to 0.012 is decreasing. Therefore, the values of the velocity distributions corresponding to small particle sizes are also reducing.

4.5. Uniformity Analysis. From the above experimental results, it can be concluded that increasing the apparent air velocity helps to improve the conveying performance of the pneumatic conveying device for particles at a constant mass flow rate. The higher apparent gas velocity can drive the particles with more incredible kinetic energy, which enhances the impact ability between the particle clusters and makes the particle clusters less likely to gather in the lifting tube. Figure 14 shows the velocity variance distribution of the particle population under different experimental conditions. The

magnitude of the variance of the particle velocities in the lifting tube implies the degree of velocity stability of the particles; the larger the variance of the particles' rates, the more unstable the particle motion. The smaller the variance value, the more uniform the velocity distribution between the particles. The velocity variance value S^2 of the particle population at U_g = 5.91 m/s is smaller at 2.08. This is because the agglomeration behavior of the particles is more severe at lower apparent gas velocities and the rates between groups of particles fluctuate more, though. However, the number of small-sized particle clusters from 0 to 0.012 was less than that in the sets of experiments with larger apparent gas velocities, thus resulting in more minor differences in particle cluster velocities. As the air velocity increases, the impact force of the airflow increases, the particle agglomerates are blown apart into small-sized particle clusters, and the velocity difference between the particle clusters gradually increases so that the velocity variance of the particle clusters, S^2, increases. The analysis of particle agglomeration size distribution for different apparent gas velocities in Figure 7 above shows that the agglomeration behavior of the particle population in the lifting tube is significantly improved when U_g > 6.91 m/s. Combined with Figure 15, when U_g > 6.91 m/s, the particle agglomerates are further blown apart into small-sized agglomerates and discrete particles, the particle distribution in the lifting tube is sparse, and the velocity difference between particles decreases. Therefore, the velocity variance S^2 has a tendency to decrease. Continuously increasing the apparent air velocity increases the forces on the particles, making the fluctuations in velocity values between particles more pronounced, as shown in Figure 14a. Therefore, when the mass flow rate at the inlet M_s = 46.50 g/s is kept constant and the apparent gas velocity U_g = 5.91 m/s, the particle distribution in the lifting tube is more homogeneous compared to the other four sets of experimental conditions, as shown in Figure 15.

Figure 16 shows the instantaneous vector velocity distribution of particles at different mass flow rates. The location of the change in reflux of particles occurs mainly at the side walls of the lift tube. At mass flow rate M_s = 16.20 g/s, the number of particles in the lifting tube is small and sparsely distributed. Currently, the lifting tube's particle cluster size is small. Still, the velocity distribution curve of the particles is

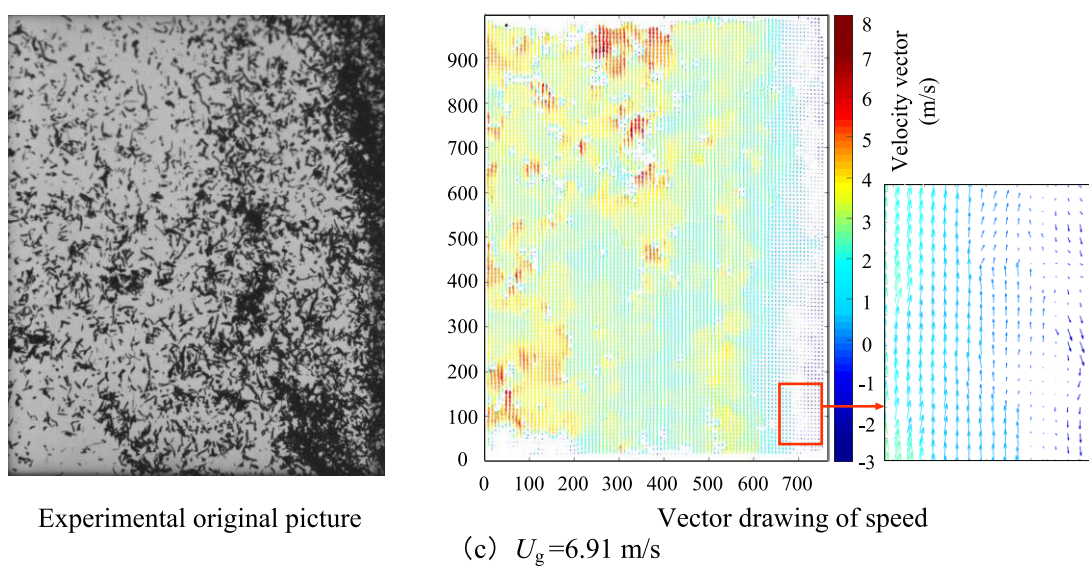Experimental original picture   Vector drawing of speed

(a) U_g =5.91 m/s

Experimental original picture   Vector drawing of speed

(b) U_g =6.40 m/s

Experimental original picture   Vector drawing of speed

(c) U_g =6.91 m/s

Figure 15. continued

(d) U_g =7.43 m/s

(e) U_g =7.91 m/s

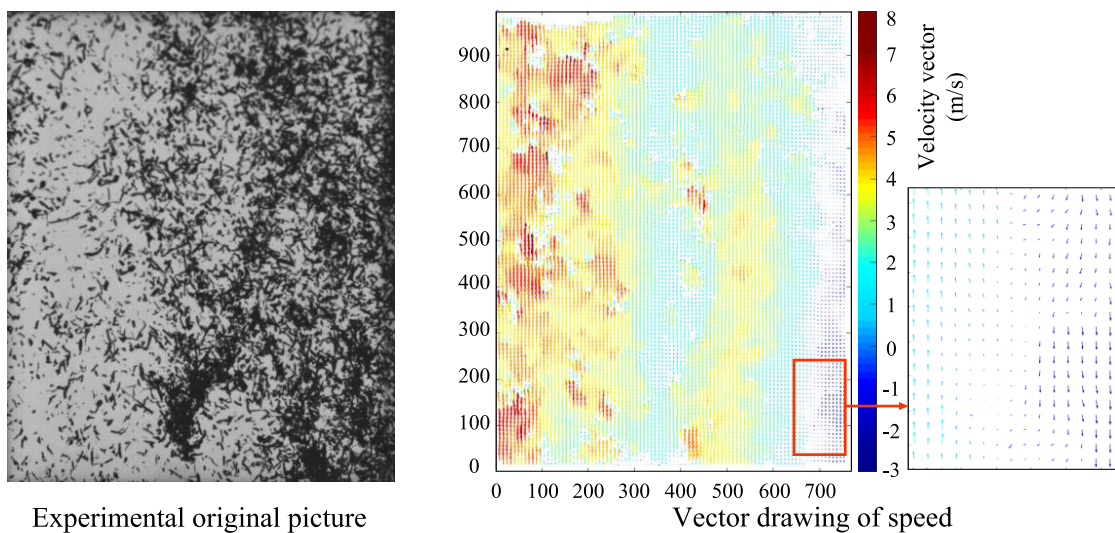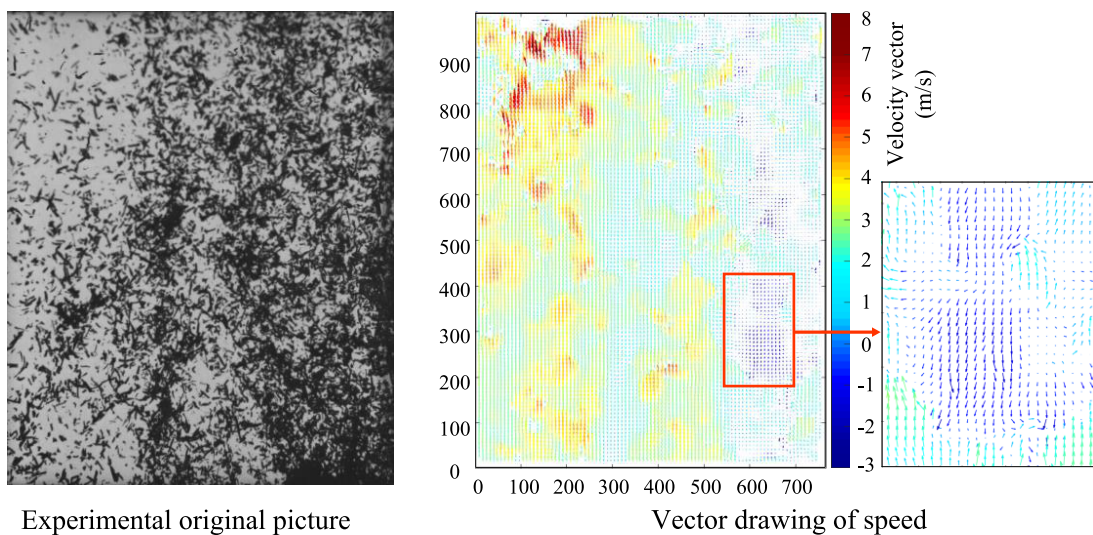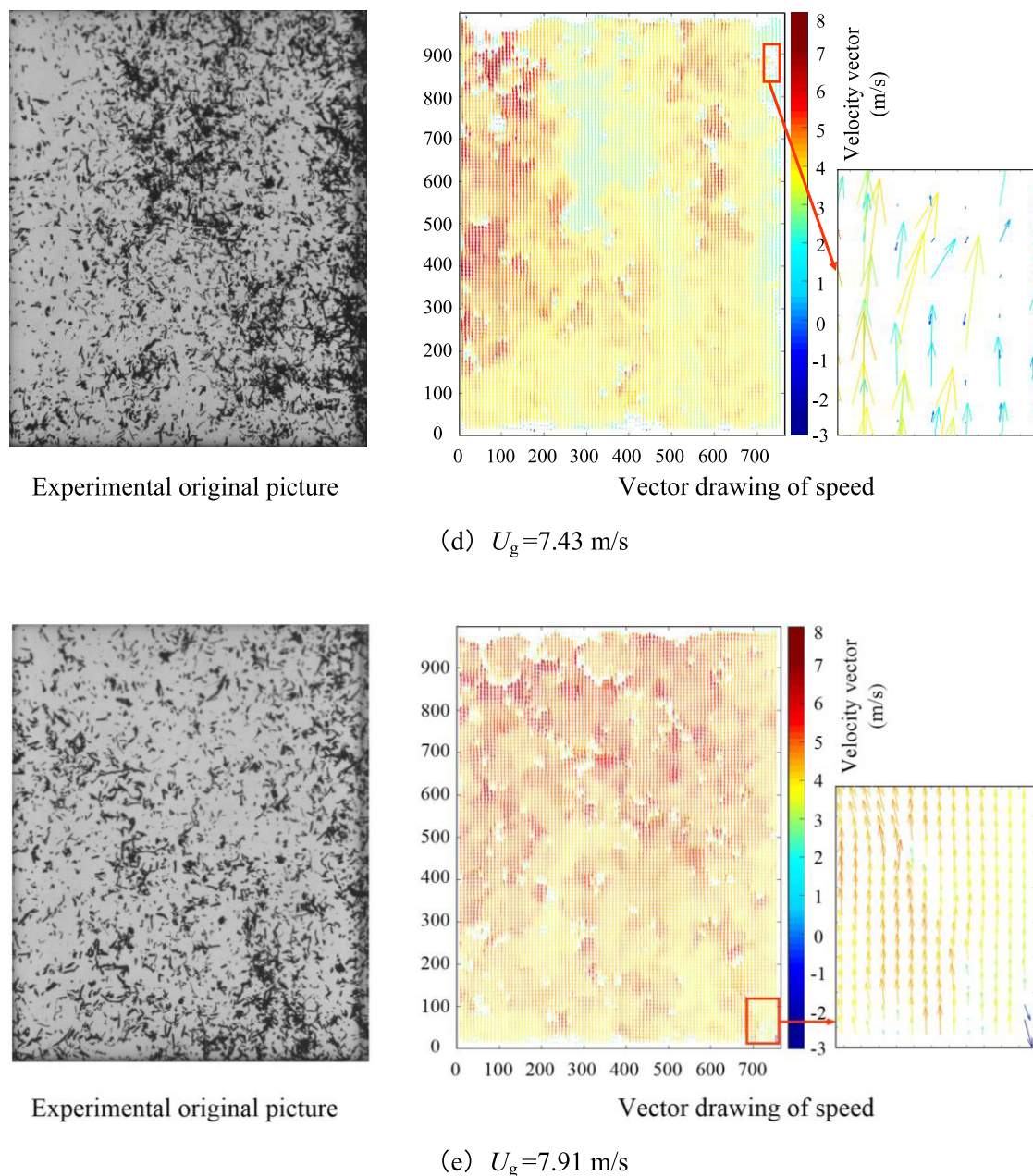**Figure 15.** Instantaneous velocity vector distribution of particles at different apparent air velocities (keep the mass flow rate constant, M_s = 46.50 g/s).

wide, and the velocity difference between the particles is significant. Therefore, this set of experiments shows that the velocity variance S^2 of the particle population is 3.55, which is the maximum value among the five sets of working conditions, as shown in Figure 14b. When M_s increased to 36.50 g/s at the inlet, the velocity variance S^2 of the particle population in the lifting tube decreased from 3.55 to a minimum value of 1.63 in the case studied in this paper. Because when M_s < 36.50 g/s, the particles in the lifting tube are very sparse, the flow field in the tube is unstable, and the velocity difference between the particles is large. When the mass flow rate is adjusted to 36.50 g/s, the movement of particles in the lifting tube is in a relatively uniform state under U_g = 6.4 m/s. And when M_s > 36.50 g/s, the agglomeration phenomenon of the particles is gradually obvious, and the velocity difference of the particles will become larger. Therefore, when M_s = 36.50 g/s, the

velocity variance S^2 in Figure 14b is the minimum value. Combining the analysis of Figure 13 with Figure 15c, it can be seen that in this set of experimental conditions, the difference in velocity between the particles in the lifting tube is slight, and the degree of reflux is also minimal compared to those of the remaining four sets of conditions. Although the maximum size of particulate agglomerates in this set of experiments was 0.464, their number was small. Significantly, these particulate agglomerates with large size were captured infrequently in all images acquired at 7s. Therefore, considering the size distribution, velocity distribution, and reflux of the particle cluster in each group of conditions, the particle population in the lifting tube is distributed more uniformly when U_g = 6.40 m/s and M_s = 36.50 g/s.

Experimental original picture   Vector drawing of speed

（a）M_s=16.20 g/s

Experimental original picture   Vector drawing of speed

（b）M_s=26.00 g/s

Experimental original picture   Vector drawing of speed

（c）M_s=36.50 g/s

Figure 16. continued

Experimental original picture

Vector drawing of speed

（d） M_s =46.50 g/s

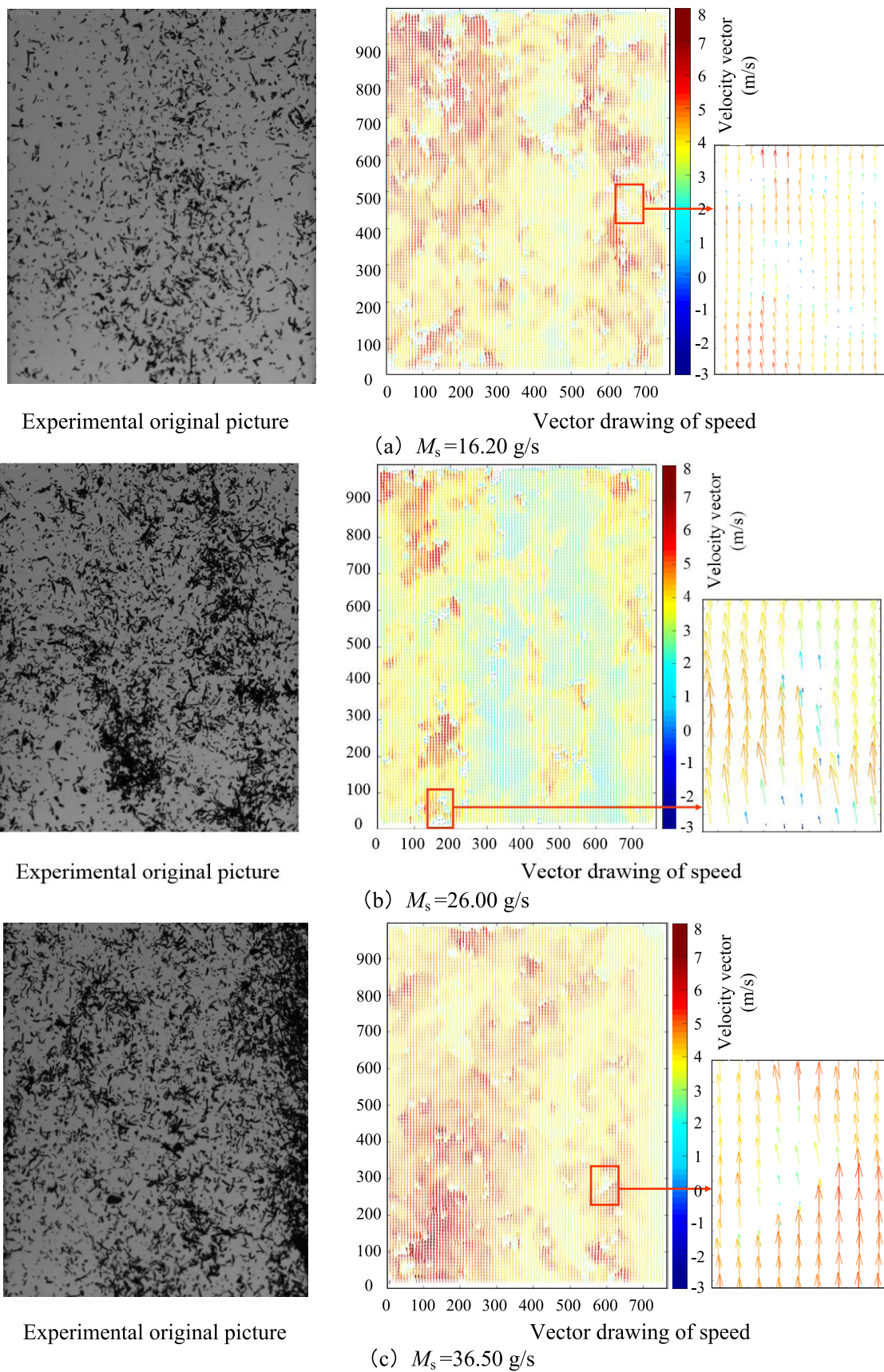Experimental original picture

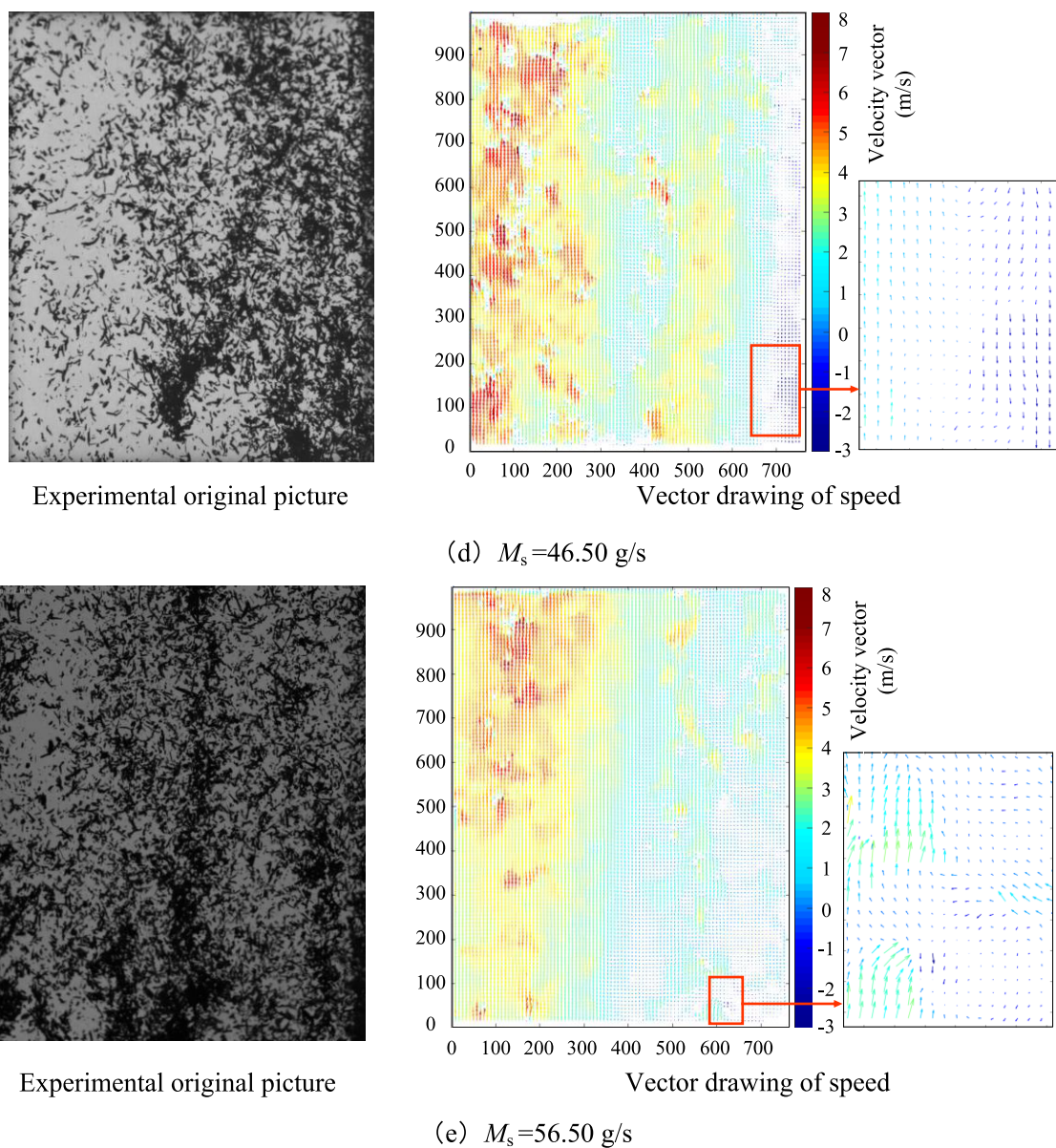Vector drawing of speed

（e） M_s =56.50 g/s

Figure 16. Instantaneous velocity vector distribution of particles at different mass flow rates (keep the apparent air velocity constant, U_g = 6.4 m/s).

5. CONCLUSIONS

The main focus of the study is the uniformity of the distribution of elongated biomass particles in the lifting tube during pneumatic conveying. Particle agglomeration and particle reflux in the pipeline can decrease the conveying performance of the pneumatic conveying system. The working conditions are adjusted through experiments to realize that the particles can be evenly distributed in the lifting tube. It is of great significance for conveying efficiency and product quality. In this article, the transport process of elongated biomass particles in the lifting tube is photographed and analyzed. The effects of apparent gas velocity and mass flow rate on transport uniformity were investigated by counting particles' size distribution and velocity distribution at different operating conditions, respectively. On the other hand, this study experimentally identified the main sites of particle agglomeration and the reasons for uneven particle motion. The phenomena and conclusions obtained in this study can help the pneumatic conveying system to improve the conveying efficiency and optimize the design and provide certain research ideas.

(1) Most elongated biomass particles exist as discrete particles in the lifting tube, but agglomeration behavior can occur. The range of cluster size corresponding to the peak in the number of clusters is mainly distributed from 0 to 0.012. It was observed that the velocity of the particles in the side wall region was significantly smaller than the velocity of the particles close to the center region, and the particles settled along the side wall with a reflux phenomenon.

(2) The apparent gas velocity U_g increased from 5.91 to 7.91 m/s, and the maximum size of agglomerates decreased from 0.689 to 0.235, while the reflux phenomenon of particles was reduced. Higher apparent gas velocities can improve the homogeneity and stability of the gas flow and reduce local velocity fluctuations and inhomogeneities, leading to a more concentrated and homogeneous particle velocity distribution.

(3) When the mass flow rate M_s at the inlet was reduced from 56.50 g/s to 16.20 g/s, the number of particles in the lifting tube decreased and the distribution became thinner. The maximum size of agglomerates decreased from 0.753 to 0.115. Therefore, with the apparent gas velocity unchanged, appropriately reducing the particle mass flow rate at the inlet can lead to better dispersion of elongated biomass particles in the lifting tube and improve the uniformity of particle distribution in the lifting tube.

(4) In several sets of conditions studied, it was found that when the apparent gas velocity was adjusted to 7.91 m/s while keeping the mass flow rate constant at 46.50 g/s, the particle population in the lifting tube was distributed more uniformly. Whereas, when the apparent gas velocity was kept at 6.4 m/s, and the mass flow rate was adjusted to 36.50 g/s, it was also observed that the return flow of the particle population in the lifting tube was less and more uniformly distributed.

■ AUTHOR INFORMATION

Corresponding Author

Conghui Gu − *School of Energy and Power, Jiangsu University of Science and Technology, Zhenjiang, Jiangsu 212100, China;* orcid.org/0000-0001-5383-2490; Email: guconghuigch@163.com

Authors

Mingpu Du − *School of Energy and Power, Jiangsu University of Science and Technology, Zhenjiang, Jiangsu 212100, China*

Junjie Yang − *China Tobacco Jiangxi Industrial Co. Ltd., Nanchang, Jiangxi 330096, China*

Ye Tao − *China Tobacco Jiangxi Industrial Co. Ltd., Nanchang, Jiangxi 330096, China*

Bingyang Xu − *China Tobacco Jiangxi Industrial Co. Ltd., Nanchang, Jiangxi 330096, China*

Haichao Zhao − *School of Energy and Power, Jiangsu University of Science and Technology, Zhenjiang, Jiangsu 212100, China*

Yuan Liu − *School of Energy and Power, Jiangsu University of Science and Technology, Zhenjiang, Jiangsu 212100, China*

Kaiyuan Deng − *School of Energy and Power, Jiangsu University of Science and Technology, Zhenjiang, Jiangsu 212100, China*

Jingyu Zhu − *School of Energy and Power, Jiangsu University of Science and Technology, Zhenjiang, Jiangsu 212100, China*

Complete contact information is available at:
https://pubs.acs.org/10.1021/acsomega.3c08719

Notes

The authors declare no competing financial interest.

■ ACKNOWLEDGMENTS

■ NOMENCLATURE

dx	transverse displacement, pixel
dy	vertical displacement, pixel
dt	time intervals, s
i	size interval
M_s	particle mass flow rate, g/s
m_1	pellet quality before drying, g
m_2	pellet quality after drying, g
φ	cluster size
S_l	cross-sectional area of lift tube, cm^2
S_{cl}	cluster size, cm^2
$n_{k_{s_i \sim s_{i+1}}}$	number of areas $S_i \sim S_{i+1}$ in a picture, piece
N_{S_i}	total number of areas $S_i \sim S_{i+1}$ in all pictures, piece
S^2	square difference of speed
S_i	area size, cm^2
t	time, s
u	lateral displacement speed, m/s
U_g	apparent gas velocity, m/s
v	longitudinal displacement speed, m/s
V	instantaneous velocity of particles, m/s
W	moisture content, %
X	background segmentation threshold

■ REFERENCES

(1) Hashemizadeh, A.; Bui, Q.; Kongbuamai, N. Unpacking the Role of Public Debt in Renewable Energy Consumption: New Insights from the Emerging Countries. *Energy* **2021**, *224*, No. 120187.

(2) Wang, Z.; Bui, Q.; Zhang, B.; Pham, T. L. H. Biomass Energy Production and Its Impacts on the Ecological Footprint: An Investigation of the G7 Countries. *Sci. Total Environ.* **2020**, *743*, No. 140741.

(3) Liu, Z.; Saydaliev, H. B.; Lan, J.; Ali, S.; Anser, M. K. Assessing the Effectiveness of Biomass Energy in Mitigating CO2 Emissions: Evidence from Top-10 Biomass Energy Consumer Countries. *Renewable Energy* **2022**, *191*, 842−851.

(4) Gu, C.; Zhang, Y.; Pan, D.; Yao, S.; Vladimir, K.; Guan, L.; Wu, K.; Yuan, Z. Visual Experimental Analysis of the Residence Time of Flexible Biomass Particles in a Baffled Rotating Cylindrical Tube. *Energy Fuels* **2020**, *34* (2), 1851−1858.

(5) Vollmari, K.; Jasevičius, R.; Kruggel-Emden, H. Experimental and Numerical Study of Fluidization and Pressure Drop of Spherical and Non-Spherical Particles in a Model Scale Fluidized Bed. *Powder Technol.* **2016**, *291*, 506−521.

(6) Zheng, C.; Zhang, L.; Govender, N.; Wu, C.-Y. DEM Analysis of Residence Time Distribution during Twin Screw Granulation. *Powder Technol.* **2021**, *377*, 924−938.

(7) Bui, Q.; Wang, Z.; Zhang, B.; Le, H. P.; Vu, K. D. Revisiting the Biomass Energy-Economic Growth Linkage of BRICS Countries: A Panel Quantile Regression with Fixed Effects Approach. *J. Cleaner Prod.* **2021**, *316*, No. 128382.

(8) Oschmann, T.; Vollmari, K.; Kruggel-Emden, H.; Wirtz, S. Numerical Investigation of the Mixing of Non-Spherical Particles in Fluidized Beds and during Pneumatic Conveying. *Procedia Eng.* **2015**, *102*, 976−985.

(9) Mondal, D. N.; Kallio, S.; Saxén, H.; Hassel, J. Experimental Study of Cluster Properties in a Two-Dimensional Fluidized Bed of Geldart B Particles. *Powder Technol.* **2016**, *291*, 420−436.

(10) Chew, J. W.; Hays, R.; Findlay, J. G.; Knowlton, T. M.; Reddy Karri, S. B.; Cocco, R. A.; Hrenya, C. M. Cluster Characteristics of Geldart Group B Particles in a Pilot-Scale CFB Riser. I. Monodisperse Systems. *Chem. Eng. Sci.* **2012**, *68* (1), 72−81.

(11) Wang, S.; Shen, Y. Coarse-Grained CFD-DEM Modelling of Dense Gas-Solid Reacting Flow. *Int. J. Heat Mass Transfer* **2022**, *184*, No. 122302.

(12) Zhou, C.; Su, J.; Jiang, X.; Shi, Z. Numerical Simulation and Experimental Verification for the Sorting Behaviors of Mixed Biomass Particles in a Novel Z-Shaped Fluidized Bed. *Chem. Eng. J.* **2022**, *441*, No. 136109.

(13) Agu, C. E.; Pfeifer, C.; Eikeland, M.; Tokheim, L.-A.; Moldestad, B. M. E. Measurement and Characterization of Biomass Mean Residence Time in an Air-Blown Bubbling Fluidized Bed Gasification Reactor. *Fuel* **2019**, *253*, 1414−1423.

(14) Gu, C.; Yao, S.; Pan, D.; Sun, S.; Guan, L.; Wu, K.; Yuan, Z. Experimental Research on the Drying Characteristics of Flexible Fibrous Biomass Fuels in the Baffled-Rotary Cylinder. *Energy Fuels* **2019**, *33* (3), 2285−2292.

(15) Li, A.; Zhu, L.; Wang, K.; Wang, G.; Wang, Z. Particles Residence Time Distribution in a Gas-Solid Cyclone Reactor Using a CFD-DDPM Tracer Method. *Powder Technol.* **2020**, *364*, 205−217.

(16) Xu, J.; Zhu, J.-X. Visualization of Particle Aggregation and Effects of Particle Properties on Cluster Characteristics in a CFB Riser. *Chem. Eng. J.* **2011**, *168* (1), 376−389.

(17) Neto, A. T. P.; Fernandes, T. C. R. L.; Da Silva Junior, H. B.; De Araújo, A. C. B.; Alves, J. J. N. Three-Phase Trickle-Bed Reactor Model for Industrial Hydrotreating Processes: CFD and Experimental Verification. *Fuel Process. Technol.* **2020**, *208*, No. 106496.

(18) Patel, A. M.; Cocco, R. A.; Chew, J. W. Key Influence of Clusters of Geldart Group B Particles in a Circulating Fluidized Bed Riser. *Chem. Eng. J.* **2021**, *413*, No. 127386.

(19) de Freitas, A. G.; dos Santos, R. B.; Riascos, L. A. M.; Munive-Hernandez, J. E.; Kuang, S.; Zou, R.; Yu, A. Experimental Design and Optimization of a Novel Solids Feeder Device in Energy Efficient Pneumatic Conveying Systems. *Energy Rep.* **2023**, *9*, 387−400.

(20) Song, J.; Wang, T.; Hu, G.; Zhang, Z.; Zhao, W.; Wang, Z.; Zhang, Y. Conveying Characteristics of Shrimp Feed Pellets in Pneumatic Conveying System and Minimum Power Consumption Dissipation Factor. *Aquac. Eng.* **2023**, *102*, No. 102347.

(21) Kong, X.; Liu, J.; Yang, T.; Su, Y.; Geng, J.; Niu, Z. Numerical simulation of feed pellet breakage in pneumatic conveying. *Biosyst. Eng.* **2022**, *218*, 31−42.

(22) Kiani, A.; Sotudeh-Gharebagh, R.; Mostoufi, N. Cluster Size Distribution in the Freeboard of a Gas−Solid Fluidized Bed. *Powder Technol.* **2013**, *246*, 1−6.

(23) Verma, S. K.; Yogi, J.; Kumar, S.; Anand, A. Experimental Investigation of Segregation in the Dilute Phase Transport of Nonspherical Particles through a Pneumatic Conveying System. *Ind. Eng. Chem. Res.* **2022**, *61*, 12776−12786.

(24) Baker, J. D.; Klinzing, G. E. Optimal performance of pneumatic transport systems. *Powder Technol.* **1999**, *104* (3), 240−247.

(25) Wu, K.; Zhang, E.; Xu, J.; Yuan, Z.; Zhu, W.; Li, B.; Wang, L.; Luo, D. Three-Dimensional Simulation of Gas-Solid Flow in a Fluidised Bed with Flexible Ribbon Particles. *Int. J. Multiphase Flow* **2020**, *124*, No. 103181.

(26) Gu, C.; Zhao, H.; Xu, B.; Yang, J.; Zhang, J.; Du, M.; Liu, Y.; Tikhankin, D.; Yuan, Z. CFD-DEM Simulation of Distribution and Agglomeration Characteristics of Bendable Chain-like Biomass Particles in a Fluidized Bed Reactor. *Fuel* **2023**, *340*, No. 127570.

(27) Zhao, H.; Xu, B.; Zhang, J.; Gu, C.; Yang, J.; Yuan, Z. Distribution characteristics of filamentous biomass particles in a rectangular lifting tube. *Acta Energ. Sol. Sin.* **2023**, *44* (09), 455−461.

(28) Liu, F.; Du, Z.; Zhu, Q.; Guo, X.; Shi, H.; Lv, P.; Li, H. Effect of High Stirring Speed on the Agglomerate Behaviors for Cohesive SiO2 Powders in Gas Fluidization. *Particuology* **2023**, *80*, 192−201.

(29) Firuzian, N.; Sotudeh-Gharebagh, R.; Mostoufi, N. Experimental Investigation of Cluster Properties in Dense Gas−Solid Fluidized Beds of Different Diameters. *Particuology* **2014**, *16*, 69−74.

(30) Wu, K.; Dai, L.; Li, B.; Gu, C.; Yuan, Z.; Luo, D. Study on Flow Characteristics of Dilute Phase Flexible Ribbon Particles in a Fluidised Bed Riser Using Particle Tracking Velocimetry. *Chem. Eng. Res. Des.* **2019**, *152*, 254−268.

(31) Wilhelm, R. H.; Kwauk, M. Fluidization of solid particles. *Chem. Eng. Prog.* **1948**, *44*, 201−218.

(32) Yerushalmi, J.; Cankurt, N. T. Further Studies of the Regimes of Fluidization. *Powder Technol.* **1979**, *24* (2), 187−205.

(33) He, Y.; Deen, N. G.; Annaland, M. V. S.; Kuipers, J. A. M. Gas−Solid Turbulent Flow in a Circulating Fluidized Bed Riser: Experimental and Numerical Study of Monodisperse Particle Systems. *Ind. Eng. Chem. Res.* **2009**, *48* (17), 8091−8097.

(34) Zha, L.; Li, J.; Cao, C.; Cao, C. S.; Huang, Y.; Zhu, H.; Liu, Z.; Zheng, C. Lattice Boltzmann simulation of three-dimensional particle group settlement. *J. Univ. Chin. Acad. Sci.* **2016**, *33*, 240−246.

(35) Deng, D.; Wang, T.; Gao, Q.; He, Y. Researches on Cluster Behaviors in a Riser Based on Clustering Algorithm. *J. Univ. Chin. Acad. Sci.* **2022**, *43*, 419−424.

(36) Wang, T.; He, Y.; Yan, S.; Tang, T.; Schlaberg, H. I. Cluster Granular Temperature and Rotational Characteristic Analysis of a Binary Mixture of Particles in a Gas−Solid Riser by Mutative Smagorinsky Constant SGS Model. *Powder Technol.* **2015**, *286*, 73−83.

(37) Liu, H.; Lu, H. Numerical Study on the Cluster Flow Behavior in the Riser of Circulating Fluidized Beds. *Chem. Eng. J.* **2009**, *150* (2−3), 374−384.

(38) Ullah, A.; Shabbir, M. B.; Umair, M.; Nadeem, M.; Xin, F. Eulerian CFD Analysis of Clustering Gas-Solid Flows in Fluidized Bed Pyrolysis Reactors. *J. Anal. Appl. Pyrolysis* **2021**, *158*, No. 105261.

(39) Sharma, A. K.; Tuzla, K.; Matsen, J.; Chen, J. C. Parametric Effects of Particle Size and Gas Velocity on Cluster Characteristics in Fast Fluidized Beds. *Powder Technol.* **2000**, *111* (1−2), 114−122.

(40) Mondal, D. N.; Kallio, S.; Saxén, H. Length Scales of Solid Clusters in a Two-Dimensional Circulating Fluidized Bed of Geldart B Particles. *Powder Technol.* **2015**, *269*, 207−218.

(41) Soong, C. H.; Tuzla, K.; Chen, J. C. Identification of particle clusters in circulating fluidized bed. *Circ. Fluid. Bed Technol.* **1994**, 615−620.

(42) Sun, Z.; Chen, D.; Zhong, W.; Yu, A. Identification and Characterization of Particle Clusters in a Fast Fluidized Bed. *J. Eng. Thermophys.* **2018**, *39*, 800−805.

(43) Shi, H.; Wang, Q.; Luo, Z.; Cen, K. PIV Measurement on the Effect of Clusters on the Gas-solid Flow Pattern in a Circulating Fluidized Bed Riser. *Chin. J. Sci. Instrum.* **2005**, 582−586.

(44) Yu, S.; Yang, X.; Xiang, J.; Li, Q.; Zhou, H.; Zhang, Y. Statistical Study of the Distribution of Voidage in a Bubbling Fluidized Bed with a Constant Section. *Chem. Eng. Res. Des.* **2021**, *171*, 305−316.

(45) Werther, J. Measurement Techniques in Fluidized Beds. *Powder Technol.* **1999**, *102* (1), 15−36.

(46) Hagemeier, T.; Börner, M.; Bück, A.; Tsotsas, E. A Comparative Study on Optical Techniques for the Estimation of Granular Flow Velocities. *Chem. Eng. Sci.* **2015**, *131*, 63−75.

(47) Lackermeier, U.; Rudnick, C.; Werther, J.; Bredebusch, A.; Burkhardt, H. Visualization of Flow Structures inside a Circulating Fluidized Bed by Means of Laser Sheet and Image Processing. *Powder Technol.* **2001**, *114* (1−3), 71−83.

(48) Wu, K.; Gao, L.; Yuan, Z.; Li, B.; Zhu, W.; Wu, Y.; Zhang, K.; Lu, D.; Luo, D. Effect of Moisture Content and Length of Flexible Filamentous Particles on Cluster Characteristics in a Fluidized Bed Dryer. *Chem. Eng. Res. Des.* **2018**, *136*, 403−416.

(49) Lu, S. Study on the Kinematic Characteristics of Fast Fluidised Bed Particle Agglomeration based on Image Method. Master's dissertation; Nanjing Normal University, 2021.

(50) Yang, J.; Zhu, J. A Novel Method Based on Image Processing to Visualize Clusters in a Rectangular Circulating Fluidized Bed Riser. *Powder Technol.* **2014**, *254*, 407−415.

(51) Yi, H.; Li, W.; Zhang, W.; Ma, L.; Yang, A. Research on Drying Characteristics of Bamboo Sawdust Fluidized Bed. *China For. Prod. Ind.* **2020**, *57*, 26−30.

(52) Yin, S.; Zhong, W.; Song, T.; Lu, P.; Chen, Y. Clusters Identification and Meso-Scale Structures in a Circulating Fluidized Bed Based on Image Processing. *Adv. Powder Technol.* **2019**, *30*, 3010−3020.

(53) Zhao, H.; Gu, C.; Xu, B.; Liu, Y.; Du, M.; Deng, K.; Zhu, J.; Voronina, I.; Yuan, Z. Numerical Analysis on the Transport Properties and Residence Time Distribution of Ribbon Biomass Particles in a Riser Reactor Based on CFD-DEM Approach. *Particuology* **2024**, *87*, 133−146.

(54) Geng, F.; Feng, X.; Teng, H.; Yuan, L.; Cai, J.; Li, T.; An, J.; Yuan, S.; Wu, S. Investigation on Dynamic Movement of Cylindrical Biomass Particles in a Fast Fluidized Bed. *Adv. Powder Technol.* **2022**, *33*, No. 103397.

(55) Chen, Y.; Lu, S.; Hu, J.; Hu, J.; Yin, S.; Song, T.; Lu, P. Structure and Development of Clusters in the Circulating Fluidized Bed Riser. *J. Nanjing Normal Univer. (Eng. Technol. Ed.)* **2020**, *20*, 15−21.